A Uccello et al.

Comparison of dust transport modelling codes in a tokamak plasma

Comparison of dust transport modelling codes in a tokamak plasma

Andrea Uccello,* Gabriele Gervasini, Francesco Ghezzi, and Enzo Lazzaro

Istituto di Fisica del Plasma "Piero Caldirola", Consiglio Nazionale delle Ricerche,
IFP-CNR, Via Roberto Cozzi 53, 20125, Milan, Italy

Minas Bacharis

Imperial College of Science and Technology, London, SW7 2AZ, UK

Joanne Flanagan and Guy Matthews

CCFE, Culham Science Centre, Abingdon, Oxon, OX14 3DB, UK

Aaro Järvinen

Aalto University, EURATOM-Tekes, 02150 Espoo, Finland

Marco Sertoli

Max-Planck-Institut für Plasmaphysik, EURATOM Association, 85748 Garching, Germany

and JET contributors

See the Appendix of F. Romanelli et al., Proceedings of the 25th IAEA Fusion Energy Conference 2014, Saint Petersburg, Russia
EUROfusion Consortium, JET, Culham Science Centre, Abingdon, OX14 3DB, UK
(Dated: March 10, 2016)

Since the installation on JET of the ITER-like Wall (ILW), intense radiation spikes have been observed, specially in the discharges following a disruption, and have been associated with possible sudden injection of tungsten (W) impurities consequent to full ablation of W dust particles. The problem of dust production, mobilization and interaction both with the plasma and the vessel tiles is therefore of great concern and requires the setting up of dedicated and validated numerical modeling tools. Among these, a useful role is played by the dust trajectory calculators, which can present in a relatively clear way qualitative and quantitative description of the mobilization and fate of selected bunches of dust grains.

CONTENTS

---

* Electronic mail: uccello@ifp.cnr.it

I. INTRODUCTION

The occurrence of Transient Impurity Events (TIEs) leading to intense radiation spikes in the Joint European Torus (JET) plasma discharges has been studied since the installation on JET of the ITER-like Wall (ILW) [1]. In JET, TIEs are most likely to occur in the discharges following a disruption [2, 3]. The measured average radiated power of 1.5 MW could be explained by a number of radiating tungsten (W) ions corresponding to the full ablation of a 100 μm-radius sphere of solid W dust [2]. A significant contribution to TIEs is also observed from iron, nickel and chromium [2, 3]. The problem of dust production, mobilization and interaction both with the plasma and the vessel Plasma-Facing Components (PFCs) is therefore important and can be articulated in few key questions:

- which are the dust initial conditions that lead to dust ablation and material deposition within the plasma?

- How much material is deposited through dust ablation in the plasma and where?

- What is the contribution of the deposited impurities to the total radiation from the plasma?

- What is the behavior of the ablated impurities in the plasma?

These issues motivate the development of dedicated and validated numerical modeling tools that can be reliably interfaced with experimental input data, for interpretative and predictive applications. Dust trajectory calculators are a useful tool to obtain in a relatively clear way a qualitative and quantitative description of the mobilization and fate of selected bunches of dust grains not interacting with one another. Two codes, DUST-TRACKing (DUSTTRACK) [4] and Dust in TOKamakS (DTOKS) [5, 6], developed at Istituto di Fisica del Plasma Milan and at Imperial College London, respectively, have been cross-tested with regard to their underlying physical models and their simulation of dust transport in JET. The main features of the codes DUST-TRACK and DTOKS are described and compared in section II, then the results of the benchmarking procedure between the two codes are presented together with selected examples from which eventually some interpretation of the TIEs basic observations could be inferred (sections III and IV). Finally some conclusions are drawn (section V).

II. DUSTTRACK AND DTOKS PHYSICS MODELS COMPARISON

In every dust simulation code available within the nuclear fusion community, the trajectories of a collection of isolated *spherical* dust particles are calculated with the aim of evaluating their distribution in the Scrape-Off-Layer (SOL) as well as their role as a source of impurities when eventually reaching the plasma region inside the separatrix. The trajectories to be computed depend both on the ambient plasma properties and on the main physical parameters of the dust particles, i.e. dust temperature T_d, surface electric potential ϕ_d (or, equivalently, the surface charge q_d) and mass M_d. The hypothesis of neglecting the interactions between different dust particles is justified for dusty plasmas with a low dust density, n_d, where the interparticle distance $\Delta \propto n_d^{-1/3} >> \lambda_d$, the Debye length. Under this assumption, the mathematical model, describing the motion of each dust particle, is a set of coupled time ordinary differential equations and/or algebraic equations. In addition to the Newton's equation of motion (by which particle position $\mathbf{x}_d$ and velocity $\mathbf{v}_d$ are calculated), both DUSTTRACK and DTOKS solve one equation for each of the dust particle parameters: T_d, ϕ_d and M_d. It follows that the physics models of such codes are comprised of the following three major elements:

1. the charging module,

2. the heating module, and

3. the active force module.

The main difference between DTOKS and DUSTTRACK is the aim to be achieved. DTOKS was developed to produce a code that is robust, flexible, and computationally inexpensive but including the essential physics for the

modeling of dust transport. DUSTTRACK is based on a more detailed physics model to the detriment of the computational speed, although maintaining the same degree of flexibility as DTOKS. These two different approaches to the problem of dust dynamics in tokamaks reflect also on the choice of the reference system where the calculations are developed. In particular, DTOKS uses a cylindrical coordinate system adequate for axisymmetric devices, like tokamaks to a first approximation. Actually, the geometry of the vessel of tokamaks is complicated by the presence of various components, such as discrete protection tiles and baffles, with recessed and protruding elements, as well as plasma diagnostics and control equipment, which can strongly influence the trajectory of the dust particles and the axisymmetric approximation no longer works. For greater simplicity of modeling in complicated geometries, DUSTTRACK assumes a three-dimensional (3D) Cartesian coordinate system and can be applied also to non-axisymmetric magnetic confinement devices (e.g. stellarators). Furthermore, the unavoidable collisions between the dust particles and tokamak PFCs can be accounted for in DUSTTRACK, while in DTOKS the grains' trajectory is terminated when they reach the wall.

In this section the charging, heating and active force physics models of DUSTTRACK and DTOKS are compared. Moreover, the reflection module implemented in DUSTTRACK is briefly described. The main features and differences of the two codes are schematically reported in table I.

II.1. The dust charging model

The dust charging module aims at the evaluation of ϕ_d, the dust particles' floating potential, which determines the fluxes of charged plasma species reaching the particles' surface, thus playing a key-role in the calculation of the forces experienced by the dust particles and ultimately their trajectories. As will be demonstrated further on, the charge models of DUSTTRACK and DTOKS well agree for negligible electron emission. When it becomes dominant instead, the two codes use very different approaches which lead to a discrepancy in the predicted values of ϕ_d.

Considering DUSTTRACK first, the charging equation is written actually for the dust charge q_d, related to ϕ_d following, in case of spherical dust particles, the well-known formula for spherical capacitors $\phi_d = q_d/(4\pi\epsilon_0 R_d)$ (where R_d is the dust particle radius and ϵ_0 is the vacuum permittivity):

$$\frac{dq_d}{dt} = I_{plasma} + I_{SEE} + I_{TI} \tag{1}$$

This equation describes the variation of the dust particle charge due to the electric currents associated to the collection of plasma charged particles (I_{plasma}) and to the emission of electrons through Secondary Electron Emission (SEE, I_{SEE}) and ThermIonic emission (TI, I_{TI}),

Feature	DUSTTRACK	DTOKS
Geometry	3D cartesian geometry	Cylindrical coordinate system
Tokamak vessel	Can include 3D features	Continuous surface
Dust-wall collisions	YES	NO
Charging model for $\delta \ll 1$	OML approach	OML approach + ambipolarity condition
Charging model for $\delta \approx 1$ and $\delta > 1$	OML approach	semi-empirical approach
Heating model	Melting/boiling/sublimation surface evaporation	Melting/boiling/sublimation
Force model	Detailed formula for the drag force	Drag force in the limit $u_s \ll 1$
Availability of tokamak plasma profiles	Full cross-section	SOL plasma fluid code mesh

TABLE I. Summary of the main features and differences of the dust simulation codes DUSTTRACK and DTOKS.

both significant in case of a thermonuclear plasma because of the high energy of the plasma species and the high energy fluxes that can heat the dust grains to high temperatures. DUSTTRACK uses different expressions for I_{plasma}, I_{SEE} and I_{TI} depending on the sign of the dust "normalized" electric potential χ_d ($= -e\phi_d k_B^{-1} T_e^{-1}$, where e is the elementary charge, k_B the Boltzmann constant and T_e the plasma electron temperature). For I_{plasma} and I_{SEE} this approach is necessary due to the electrostatic nature of the interactions between plasma species and dust surface charges. Moreover, as I_{SEE} and I_{TI} are concerned, when the dust particle is positively charged ($\chi_d < 0$), some secondary and thermionic electrons are pulled back and recollected by the dust grain.

In order to evaluate I_{plasma}, DUSTTRACK relies on the Orbital Motion Limited (OML) approach for spherical dust particles [7, 8], which is a good approximation for small grains compared with the Debye length. The I_{SEE} term is well described through the δ_{SEE} yield, which corresponds to the number of secondary electrons the dust grain emits when it is hit by an electron (no other colliding species are considered). It is a function of the impinging electron energy and incidence angle. δ_{SEE} is assumed separable with respect to these two variables. The dependance on energy at normal incidence is modeled with the Kollath's semi-empirical formula [9]. The angular part is treated following [10]. In order to find I_{SEE}, δ_{SEE} is numerically integrated over the hypothesized Maxwellian energy distribution of incoming electrons. When $\chi_d < 0$ ($q_d > 0$), some secondary electrons are eventually trapped and recollected by the dust. Such electrons do not contribute to I_{SEE} and a corrective factor is included [11]. The thermionic current I_{TI} is expressed through the Richardson-Dushman formula [12] properly modified to take into account the Schottky effect for $q_d < 0$ and the fraction of the emitted electrons pulled back to the dust grain when $q_d > 0$, which is not considered in the evaluation of I_{TI} [13] (as in the case of I_{SEE}).

Moving on to DTOKS, it uses a different approach to the problem of dust charging with respect to DUST-TRACK. DTOKS considers two different dust charge equations depending on the value of the total electron yield δ ($= \delta_{SEE} + \delta_{TI}$), defined as the ratio of the flux of the emitted electrons from the dust surface over the flux of the impinging electrons from the plasma [6]. For $\delta \ll 1$, it is expected that the dust particle would remain negatively charged and the effect of the emitted electrons to its potential would be negligible. In this case, DTOKS solves equation 1 applying the ambipolarity condition $dq_d/dt = 0$, which is based on the very small charging time of the dust grain in the tokamak plasmas. As DUSTTRACK, DTOKS evaluates I_{plasma} by means of the OML approach. Considering the emission mechanisms, δ_{SEE} is calculated from a logarithmic equation for the plasma electron temperature T_e, and the thermionic current is modeled with the Richardson-Dushman formula but the Schottky effect is not considered [6]. The main difference between the DTOKS charging model and the one implemented in DUSTTRACK is how they treat the cases of dominant electron emission, $\delta \approx 1$ and $\delta > 1$, where in DUSTTRACK there might be a positively charged dust grain. DTOKS assumes the formation of a potential well around the dust particle and includes its impact using a semi-empirical model (the emitted population of electrons acts like "shielding" the positively charged dust grain from the electrons of the plasma). This was motivated by particle-in-cell analyses [14, 15] that demonstrate a departure from the typical dust particle Debye-Hükel-like potential and the formation of a potential well around the grain under such conditions. So, for plasma collection purposes (i.e. for the evaluation of I_{plasma}), even when $\delta \approx 1$ and $\delta > 1$, in DTOKS the dust particle has a negative potential with respect to the plasma background. In contrast with DUSTTRACK, which always uses equation 1 to compute the dust electric potential, in DTOKS ϕ_d for $\delta \approx 1$ and $\delta > 1$ is calculated by OML with a correction due to the depth of the potential well (for more details, see [6] and references therein).

Since approximately the $\chi_d > 0$ ($\chi_d < 0$) "regime" of DUSTTRACK coincides with the $\delta \ll 1$ ($\delta \approx 1$ and $\delta > 1$) "regime" of DTOKS, a direct comparison between the charging models of the two codes is possible investigating for example the behavior of χ_d as a function of the dust temperature T_d (which regulates the importance of I_{TI} with respect to the other currents and finally determines the value of δ). Figure 1 shows $\chi_d(T_d)$ for a spherical tungsten dust particle immersed in a background deuterium plasma with electron and ion temperatures of $T_e = T_{D^+} = 10$ eV and electron density $n_e = 10^{18}$ m^{-3}, which flows with a relative velocity of 400 m/s with respect to the dust particle. In the case of DUSTTRACK,

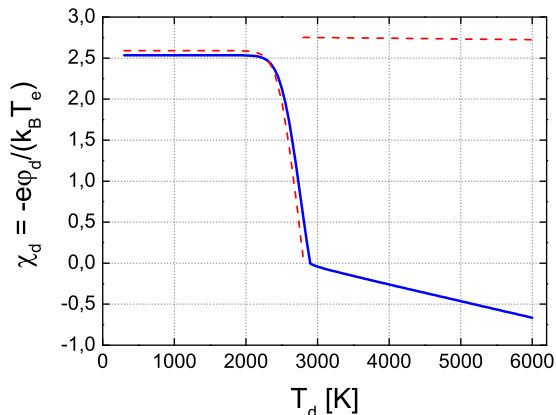FIG. 1. Plot of the dust normalized potential χ_d as a function of the dust temperature T_d for a spherical W dust particle immersed into a deuterium plasma with $T_e = T_{D^+} = 10$ eV and $n_e = 10^{18}$ m^{-3}, flowing with a relative velocity of 400 m/s with respect to the dust particle, as calculated by DUST-TRACK (solid blue line) and DTOKS (dashed red line). Both SEE and TI emission are included in the calculation.

the $\chi_d(T_d)$ relation is evaluated imposing the ambipolarity condition to equation 1. As expected, the main difference between the lines in figure 1 is in the region of the high temperatures where the thermionic emission takes a key-role in the charging process, leading to $\delta \approx 1$ and $\delta > 1$. Here, the shielding effect of dust particle positive potential due to the emitted electron population, described semi-empirically in DTOKS, sets up. For DUSTTRACK instead, the shallow corrective factors of the SEE and TI terms reduce the dust particle potential practically to zero (it becomes just slightly positive for high temperatures). The inclusion of a more suitable shielding model (like that of DTOKS) for $\chi_d < 0$ in DUSTTRACK is ongoing.

II.2. The dust heating model

The heating module allows to evaluate the power absorbed by the dust grain (Q_{tot}), which plays a major role in the variation of the dust particle temperature T_d, thus governing possible phase transitions (i.e. subli-

mation, melting, boiling and surface evaporation), ultimately responsible for the occurrence of TIEs. Considering the heating process isobaric, both DUSTTRACK and DTOKS equate Q_{tot} to the rate of change of dust particle enthalpy H_d ($dH_d/dt = M_d c_{p,d} T_d$, where $c_{p,d}$ is the specific heat at constant pressure of the dust material). The first contribution to Q_{tot} is the kinetic energy flux to the dust grain due to its bombardment with the different (charged and neutral) species s of the background plasma: Q_s. Both codes evaluate Q_s in the frame of the OML approach. In particular, during computation, DUSTTRACK assumes a drifting Maxwellian distribution for ions and neutrals and a stationary Maxwellian distribution for electrons. DTOKS, instead, neglects the contribution from the neutral species and considers a stationary Maxwellian distribution for the electrons and the different ion populations [6].

The other terms of Q_{tot} modeled both by DUST-TRACK and DTOKS are the powers associated to secondary electron, thermionic and black-body emissions (Q_{SEE}, Q_{TI}, Q_{rad}, respectively). The latter is described by the Stefan-Boltzmann law. Considering the secondary electron and thermionic emissions, DUSTTRACK integrates the flux of emitted electrons over their energy distribution. Q_{SEE} is evaluated using the energy distribution of [11] and the TI electrons are modeled through a Maxwellian distribution with the dust temperature T_d. The energy needed for the initial release of the electrons, i.e. the work function of the dust material, is also taken into account. DTOKS evaluates Q_{TI} in the same way as DUSTTRACK and for the SEE assumes monoenergetic secondary electrons with energy of 3 eV [6]. Moreover, DTOKS calculates the power associated to the ion backscattering mechanism and neutral recombination [5, 6], which DUSTTRACK does not consider.

Because of the really high temperatures in the near-SOL, dust particles undergo bulk phase transitions (i.e. sublimation, melting and boiling) rather quickly approaching the separatrix. Due to the small pressure inside the tokamak chamber (e.g. $1 \div 10$ Pa in the divertor region of ITER [16]), also dust surface evaporation, whose impact on the dust mass decrease becomes strong from temperatures of the order of some thousand of K for typical plasma-facing materials, may play a significant role. DUSTTRACK and DTOKS heating modules are therefore completed with suitable phase transition models. Both codes consider sublimation, melting and boiling, while surface evaporation is accounted for only in DUSTTRACK, through the Hertz-Knudsen formula [17]. In this case the mass loss rate of the dust particle is proportional to its vapor pressure which is strongly temperature and material dependent. The phase transition models of DUSTTRACK and DTOKS rely on the following assumptions: (i) dust grain always retains its spherical shape and (ii) the dust particle mass loss channels are the gas phase transitions. Since the mass loss due to gas phase transitions also corresponds to a loss of power, DUSTTRACK includes this quantity (Q_{gas}, evaluated as the sum of the power that the cloud of gaseous matter

had as a part of the dust particle and the power necessary to gasify its mass) to the computing of the net power reaching the dust particle, Q_{tot}. This contribution is not present in DTOKS.

Finally, DTOKS considers the main thermodynamic properties of the dust materials constant with the temperature. In DUSTTRACK, the dependence on T_d of the enthalpy, specific heat, vapor pressure, etc., is introduced by means of suitable polynomial fits of tabulated experimental values [18, 19].

II.3.   The dust active forces model

The active force module of both DUSTTRACK and DTOKS, which determines the trajectories of the test dust particles, is based on the Newton's equation of motion. The total force to which a dust particle is subject to comprises of the friction forces due to the interaction with the plasma species (because of their tiny mass, electrons are neglected in the momentum transfer process), indicated with $\mathbf{F}_{drag}$, the Lorentz force $\mathbf{F}_{Lorentz} = q_d(\mathbf{E} + \mathbf{v}_d \times \mathbf{B})$ (where $\mathbf{v}_d$ is the dust particle velocity - v_d indicates its magnitude in the following - $\mathbf{E}$ and $\mathbf{B}$ are the electric and magnetic fields) and the gravitational force $M_d\mathbf{g}$. In case of ferromagnetic dust grains, DUSTTRACK evaluates the force $\mathbf{F}_{\nabla \mathbf{B}}$ [4] which describes the interaction between the dust particle magnetic dipole and the ambient magnetic field $\mathbf{B}$. This term is not modeled by DTOKS. Although $\mathbf{F}_{\nabla \mathbf{B}}$ is subdominant (with respect to the drag force) in the SOL, it is important for both mobilizing the dust stuck on the tokamak vessel wall on the low-field side, and in favoring trapping close to the wall on the high-field side [4].

In the binary collision approach, the drag force due to the charged species $\mathbf{F}_{drag}$ can be separated in two terms, the first due to their absorption by the dust grain ($\mathbf{F}_{coll}$, collection drag force) and the second due to small-angle Coulomb collisions with closely orbiting plasma particles ($\mathbf{F}_{orb}$, orbital drag force) [20]. DUSTTRACK also evaluates the force associated to the absorption by the dust particle of the neutral species of the plasma (e.g. deuterium atoms). DTOKS considers instead only the charged species.

Since it has been demonstrated (figure 7 in [6]) that the drag force has a dominant influence on dust particle trajectories, the expressions of $\mathbf{F}_{coll}$ and $\mathbf{F}_{orb}$ implemented in the two codes will be reported and the differences highlighted. Both DUSTTRACK and DTOKS evaluate the collection drag force on the basis of the cross sections of the OML theory and its refinements [5–7, 20–23]. Specifically, DUSTTRACK uses the approach reported in [20] which leads to the following formula for the collection drag force due to the ion species s (with mass m_s, charge Z_s, density n_s, temperature T_s and flow velocity $\mathbf{v}_{s,drift}$):
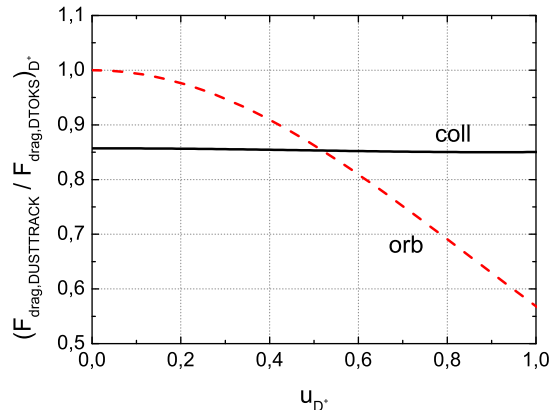

FIG. 2.   Plot of the ratio between the collection drag force (solid black line) implemented in DUSTTRACK and in DTOKS as a function of u_{D+}, for a deuterium plasma with $T_e = T_{D+} = 10$ eV impinging on a dust particle with $\chi_d = 2.5$. Plot of the ratio between the orbital drag force (red dashed line) of DUSTTRACK and DTOKS as a function of u_{D+}. The practical range is that for which $u_{D+} < 0.5$. For clarity the plot is up to $u_{D+} = 1$; for $u_{D+} > 1$ the ratio between the collection drag forces departs from 1.

$$\mathbf{F}_{s,coll}^{\chi_d \leq 0} = \pi R_d^2 m_s n_s v_{T_s} (\mathbf{v}_{s,drift} - \mathbf{v}_d) \frac{1}{4u_s^2} \left\{ \frac{1}{\sqrt{\pi}} \right.$$

$$\cdot \left[\left(1 + 2u_s^2 + \frac{1 - 2u_s^2}{u_s} \sqrt{-\frac{Z_s \chi_d}{\tau_s}} \right) \exp\left(-u_{s+}^2\right) \right.$$

$$\left. + \left(1 + 2u_s^2 - \frac{1 - 2u_s^2}{u_s} \sqrt{-\frac{Z_s \chi_d}{\tau_s}} \right) \exp\left(-u_{s-}^2\right) \right]$$

$$+ u_s \left[1 + 2w_{s+} - \frac{1}{2u_s^2} (1 - 2w_{s-}) \right]$$

$$\left. \cdot \left[\mathrm{erf}\left(u_{s+}\right) + \mathrm{erf}\left(u_{s-}\right) \right] \right\}$$

$$\tag{2}$$

$$\mathbf{F}_{s,coll}^{\chi_d > 0} = \pi R_d^2 m_s n_s v_{T_s} (\mathbf{v}_{s,drift} - \mathbf{v}_d)$$

$$\cdot \frac{1}{2u_s^2} \left\{ \frac{1}{\sqrt{\pi}} (1 + 2w_{s+}) \exp\left(-u_s^2\right) \right.$$

$$\left. + u_s \left[1 + 2w_{s+} - \frac{1}{2u_s^2} (1 - 2w_{s-}) \right] \mathrm{erf}\left(u_s\right) \right\}$$

$$\tag{3}$$

$v_{T_s} = \sqrt{2k_B T_s/m_s}$ is the thermal velocity of the plasma species s, $\tau_s = T_s/T_e$ is the species' normalized temperature with respect to the electron temperature, $u_s = |\mathbf{v}_{s,drift} - \mathbf{v}_d|/v_{T_s}$ is the species' normalized flow velocity (in the reference system of the dust particle) to its thermal velocity. $u_{s\pm} = u_s \pm \sqrt{-Z_s \chi_d/\tau_s}$ and $w_{s\pm} =$

$u_s^2 \pm Z_s \chi_d / \tau_s$. DTOKS, instead, evaluates the collection ion drag force in the limit $u_s \ll 1$, following [21]

$$\mathbf{F}_{s,coll} = 2\sqrt{\pi} R_d^2 m_s n_s v_{T_s} (\mathbf{v}_{s,drift} - \mathbf{v}_d) \left(1 + \frac{\chi_d}{\tau_s}\right) \quad (4)$$

In order to directly compare the expressions of $\mathbf{F}_{s,coll}$ implemented in the two codes, the ratio between Eq. 3 and Eq. 4 has been calculated and plotted in figure 2 (solid black line) as a function of the normalized species flow velocity with respect to its thermal velocity u_s, for a deuterium plasma with ions and electrons temperature of 30 eV impinging on a dust particle with the typical normalized electric surface potential of $\chi_d = 2.5$ (see figures 6g-h). From figure 2, the ratio remains constant for normalized flow velocity of deuterium ions ($s = D^+$) $0 \leq u_{D^+} \leq 1$. According to expectation, the ratio diverges when the flow velocity of deuterium ions exceeds their thermal velocity (not shown in figure 2). In the limit of validity of Eq. 4, for $u_{D^+} \ll 1$, despite DUSTTRACK and DTOKS following different approaches to evaluate the collection drag force (contained in [20] and [21], respectively), the discrepancy between the two codes stays within 15% and the agreement between the two codes thus appears quite satisfactory.

Moving on to the orbital part of the drag force, DUST-TRACK and DTOKS evaluate $\mathbf{F}_{orb}$ through the expressions reported in [20] and [24], respectively. Both formulas can be rewritten using the following common form:

$$\begin{aligned} \mathbf{F}_{s,coll} =& 2\pi n_s m_s v_{T_s} (\mathbf{v}_{s,drift} - \mathbf{v}_d) \\ & \cdot R_d^2 \left(\frac{Z_s \chi_d}{\tau_s}\right)^2 \Lambda_s \frac{G(u_s)}{u_s} \end{aligned} \quad (5)$$

where Λ_s is the modified Coulomb logarithm, $-\exp(\beta_{T,s}/2) Ei(-\beta_{T,s}/2)$, Ei is the exponential integral, $\beta_{T,s}$ is the thermal scattering parameter: $\beta_{T,s} = R_d |\chi_d| / (\tau_s \lambda_s)$. λ_s is the effective screening length (see reference [24]). The difference between the two codes is how they treat the term $G(u_s)$: the Chandrasekhar function [25]. DUSTTRACK implements it in full. DTOKS uses its approximation in the limit of $u_s \ll 1$, $G(u_s) \approx 2u_s/(3\sqrt{\pi})$.

Referring to the red dashed line of figure 2, which shows the ratio of the orbital drag force implemented in DUSTTRACK and in DTOKS, the agreement between the two codes is good till $u_{D^+} \approx 0.5$. For higher values of the flow velocity, DTOKS starts to overestimate the orbital drag force. Contrary to the ratio of the collection drag forces, since the Chandrasekhar function depends only on u_s, the ratio of the orbital drag forces does not depend on plasma and dust particle properties.

In DUSTTRACK, the implementation of the full expressions for the collection and orbital drag forces (valid also for $u_s \approx 1$ and $u_s > 1$) allows one to describe peculiar phenomena like the hyper-velocity ($u_s \propto v_d$) of some dust particles in particular conditions of plasma, PFCs and dust material [26].

II.4. Dust-wall collisions in DUSTTRACK

DTOKS does not consider the interactions between dust particles and PFCs, while DUSTTRACK relies on a very flexible reflection module. Since an appropriate time-scale for collisions is of the order of tens of ns [27] and the typical time-steps used in DUSTTRACK are fraction of μs, the interactions are modeled through an impulsive force which leads to a discontinuous change of the particle velocity [27, 28]. In its lightest version, the reflection model describes perfectly elastic mirror-like reflections. In its comprehensive version (dust particles-wall collisions are also fully treated by the MIGRAINe code [27–29]), it includes inelastic effects and also the consideration of PFCs surface roughness (at the μm-scale) through a randomization of the direction vector of the dust particle after the reflection from the vessel, sampling from a cosine distribution (this approach is different from the one adopted in MIGRAINe). The inelastic character of the interactions is treated starting from the approach of C. Thornton and Z. Ning [28, 30]. Normal and tangential restitution coefficients model the dust grain velocity loss after the collision [31–34]. Moreover, the normal reflection velocity of the dust particles must exceed a certain value called "sticking velocity", below which no rebound occurs. Following [30], the value of this critical velocity depends on the mechanical properties of the materials involved in the impact, and on the radius of the impinging particle [28]. Here, in this context, the sticking velocity is a constant parameter taken from empirical values.

III. TRANSPORT OF A CARBON DUST PARTICLE IN A UNIFORM AND CONSTANT HYDROGEN PLASMA

In this section, a first comparison between the outputs of DUSTTRACK and DTOKS is reported. The two codes are applied to the very simple case described in [5]: a carbon 5 μm-radius dust particle injected upward (at initial temperature $T_{d,i} = 300K = RT$, Room Temperature) into a uniform hydrogen plasma background flowing perpendicular to it. The input parameters of the test (the "reference" case hereafter) are summarized in table II.

Since no electric and magnetic fields are present and the dust particle is not ferromagnetic, the total force to which the carbon grain is subject to is comprised only by the drag and the gravitational forces. $\mathbf{F}_{drag}$ (which is concordant with $\mathbf{v}_{H^+,drift}$) dominates $M_d \mathbf{g}$ forcing the dust particle to turn to the direction of the hydrogen plasma flow.

Starting from the "reference" case of table II, a sensitivity study, whose results are in part already reported in [5] for DTOKS, was also made for DUSTTRACK. The response of the lifetime and distance travelled by the dust particles was evaluated relative to variations of key parameters. The latter are: plasma electron temperature

$T_e = T_{H+}$	$n_e = n_{H+}$	$v_{H+,drift}$	$v_{d,i}$	$\alpha_{H+,drift-d,i}$	$R_{d,i}$	$T_{d,i}$
30 eV	2×10^{19} m^{-3}	400 m/s	10 m/s	90°	5 μm	300 K

TABLE II. Input "reference" parameters of the comparative case. The carbon dust particle is launched upward (@RT) with initial velocity $v_{d,i}$ necessary to overcome the adhesion force. The plasma flows perpendicular to the dust grain (angle between $\mathbf{v}_{H+,drift}$ and $\mathbf{v}_{d,i}$: $\alpha_{H+,drift-d,i}$, is 90°).

(T_e) and number density (n_e), and the magnitude of the ion drag force ($|\mathbf{F}_{drag}|$). The results are summarized in figure 3 which shows the behavior of the distance travelled by the dust grain horizontally, $|D_x|$ (figure 3a), and of its lifetime, Δt (figure 3b), as a function of the ratio of the parameter considered (T_e, n_e and $|\mathbf{F}_{drag}|$) to its reference value (table II). The sensitivity investigation made on DUSTTRACK (solid lines) and DTOKS (dashed lines) gives the same qualitative behavior but the estimated values of $|D_x|$ and Δt are in general very different. The decrease of $|D_x|$ and Δt increasing T_e and n_e is expected because their increase results in higher heating fluxes to the dust grain and a reduction of its travelled distance and lifetime. Comparatively to the effects of plasma background changes, the ion drag force has a shallow impact on $|D_x|$ and Δt. In particular, the horizontal travelled distance increases almost linearly with $|\mathbf{F}_{drag}|$. This is because the action of the ion drag in this direction accelerates the dust particle (plasma flows horizontally).

The origin of the discrepancy between the values of $|D_x|$ and Δt predicted by the two codes, apparent from figure 3, cannot be attributed to the different expressions for the drag force implemented in DUSTTRACK and DTOKS (see subsection II.3) since $u_{H+} \ll 1$ always in this case. It is instead principally due to the fact that DUSTTRACK, unlike DTOKS (see table I), contemplates the surface evaporation as a channel of dust particle mass loss. As a proof of this, consider the behavior of $|D_x|$ and Δt with the plasma electron temperature T_e. For the lower values of T_e, the temperature of the carbon grain T_d calculated by DUSTTRACK hardly reaches the sublimation point (or anyway sufficiently high temperatures to make the mass loss due to surface evaporation important) for the cooling effect of the surface evaporation (expressed by Q_{gas} in the power balance of the heating module, subsection II.2). In the case of $T_e/T_{e,ref} = 50\%$, DUSTTRACK estimates $|D_x|$ and Δt 3 and 2 orders of magnitude higher than the values predicted by DTOKS. For the higher values of T_e, T_d rapidly tends to the sublimation temperature causing a just as fast reduction of the dust particle mass. The surface evaporation plays a marginal role here. Within this regime, i.e. at $T_e/T_{e,ref} = 125\%$ and 150%, this leads to a good quantitative agreement between the values of $|D_x|$ and Δt estimated by the two codes.

To further demonstrate that the responsible of the discrepancy between the values of the dust particle travelled distance and lifetime predicted by the two codes is the surface evaporation, the sensitivity study made on DUSTTRACK was repeated switching off the phase transitions module (no surface evaporation and sublimation are included into the description: the simulations ended when the dust particle reached the sublimation point). The results are plotted in figure 4. The qualitative and quantitative agreement of the behaviors of $|D_x|$ and Δt with T_e, n_e and $|\mathbf{F}_{drag}|$ computed by the two codes has become better except for an offset due to the fact that sublimation was not described by DUSTTRACK here.

IV. APPLICATION OF DUSTTRACK AND DTOKS TO A JET PULSE

Among the possible applications of the results of the dust transport simulation codes, the interpretation of the physics underlying TIEs is one of the most interesting. In JET, TIEs have been systematically investigated since the installation of the ILW and a possible hypothesis of their occurrence is the full ablation of a solid W dust particle some tens of μm in radius [2]. The evaluation of the trajectories of the dust particles, together with the distribution of the ablated mass during their flight, should allow in principle some indirect crosscheck with existing diagnostics such as fast camera tracers, impurity spectroscopy and high resolution Thomson scattering techniques, shedding more light on the phenomenon of TIEs. Having this final purpose in mind, the last step of the comparative procedure was the application of DUSTTRACK and DTOKS to a JET pulse (#82806 at 55-56 s; the background plasma was modeled through EDGE2D-EIRENE [35, 36]) to investigate the dynamics of W spherical dust particles with 10 μm-radius produced from JET divertor region. Four W particles were launched from the outer divertor, with an initial speed $v_{d,i}$ of 10 m/s (necessary to overcome the adhesion force) and different input angles. Ambient plasma and dust particle main parameters are reported in table III. The comprehensive version of DUSTTRACK reflection module (i.e. inelastic collisions and consideration of tiles surface roughness through a randomization of the direction vector of the dust particle after the reflection from PFCs, subsection II.4), with and artificial sticking velocity of 1 m/s, was used.

A substantial difference between the two codes when they are applied to tokamaks is related to the input information, i.e. the profiles of the ambient plasma properties typically available on SOL plasma fluid transport codes (EDGE2D here) meshes. The latter usually do not extend to the tokamak vessel, therefore referring to a belt region across the separatrix and the SOL layer. Nevertheless, the volume outside the SOL is a region
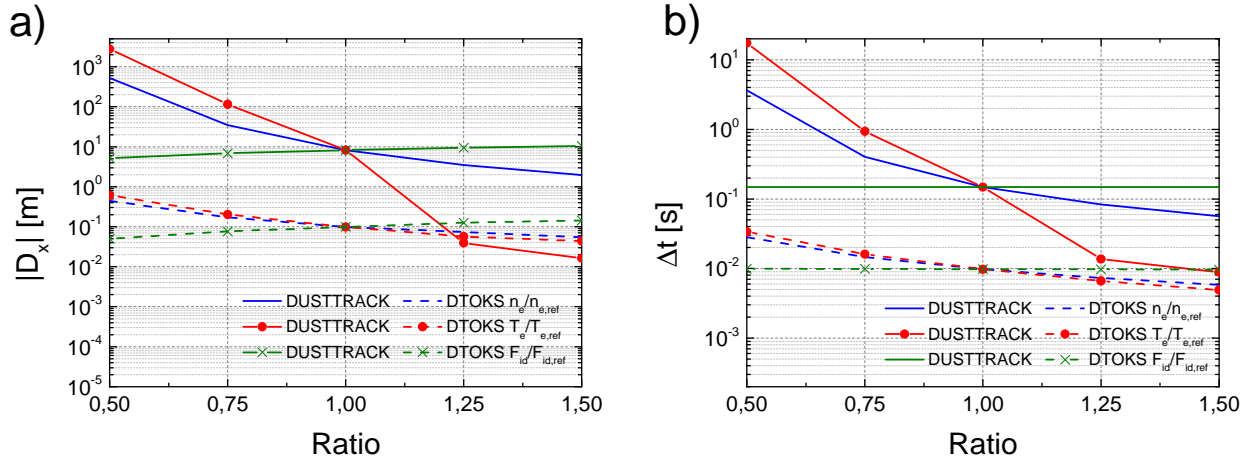
FIG. 3. Plot of the distance $|D_x|$ travelled horizontally by the dust grain (a), and of the dust lifetime Δt (b), as a function of the ratio of the corresponding parameter (i.e. T_e, n_e, $|\mathbf{F}_{drag}|$) to its reference value (see table II). Solid and dashed lines are used for DUSTTRACK and DTOKS results, respectively.
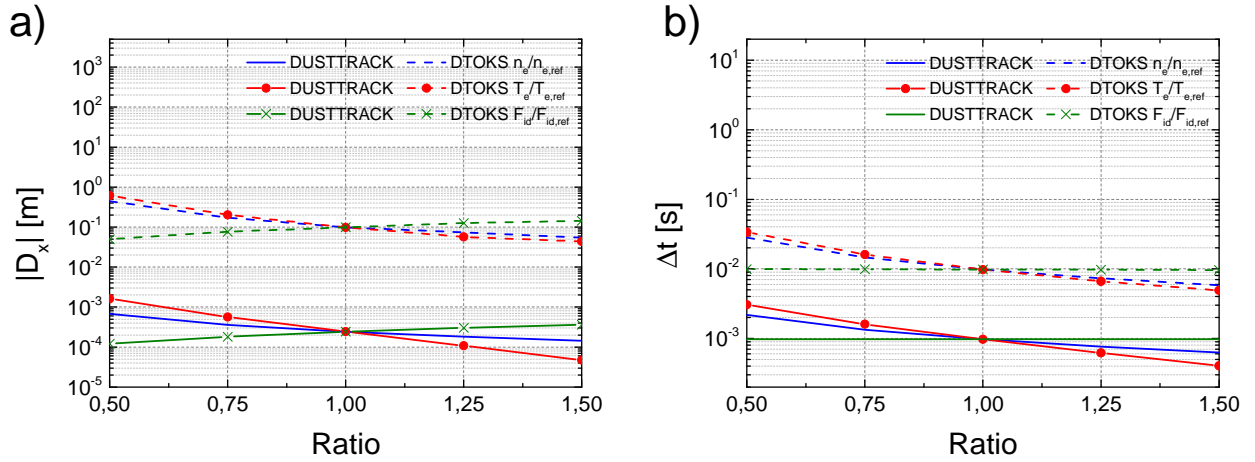

FIG. 4. Plot of $|D_x|$ (a) and Δt (b), as a function of the ratio of the corresponding parameter to its reference value. Here, surface evaporation and sublimation are not included in DUSTTRACK. Solid and dashed lines are used for DUSTTRACK and DTOKS results, respectively.

$T_{e,sep}$	$T_{i,sep}$	$n_{e,sep} = n_{i,sep}$	$v_{d,i}$	$R_{d,i}$	$T_{d,i}$
387 eV	$T_{e,sep} \times 1.6$	0.948×10^{19} m^{-3}	10 m/s	10 μm	300 K

TABLE III. Representative input parameters of DUSTTRACK and DTOKS for JET shot #82806 at 55-56 s. $T_{e(i),sep}$ and $n_{e(i),sep}$ are plasma electron (ion) temperature and density on the separatrix at the outer midplane, respectively. Tungsten dust particles were launched with initial velocity $v_{d,i}$ and different input angles from JET outer divertor. The initial temperature $T_{d,i}$ is also specified.

where dust particles can spend part of their life and tiles not intersecting the magnetic field lines can anyway constitute places for dust deposition. For these reasons, DUSTTRACK performs a numerical extrapolation of the plasma profiles to the vessel using an inverse distance weighting Shepard's method [37]. DTOKS, instead, makes the approximation of considering the space between the SOL codes meshes and the tokamak vessel as a vacuum region.

In figure 5 the trajectories of the four W dust particles starting from the outer divertor, predicted by DUST-TRACK (solid lines) and DTOKS (dotted lines) are shown. For readability reasons, the results are presented considering separately the particles that go toward the separatrix (#1 and #2, figure 5a) and those that encounter the wall during their motion (#3 and #4, figure 5b). Figure 6 also reports the evolution of the main parameters of the simulated dust grains: T_d (a-b), R_d
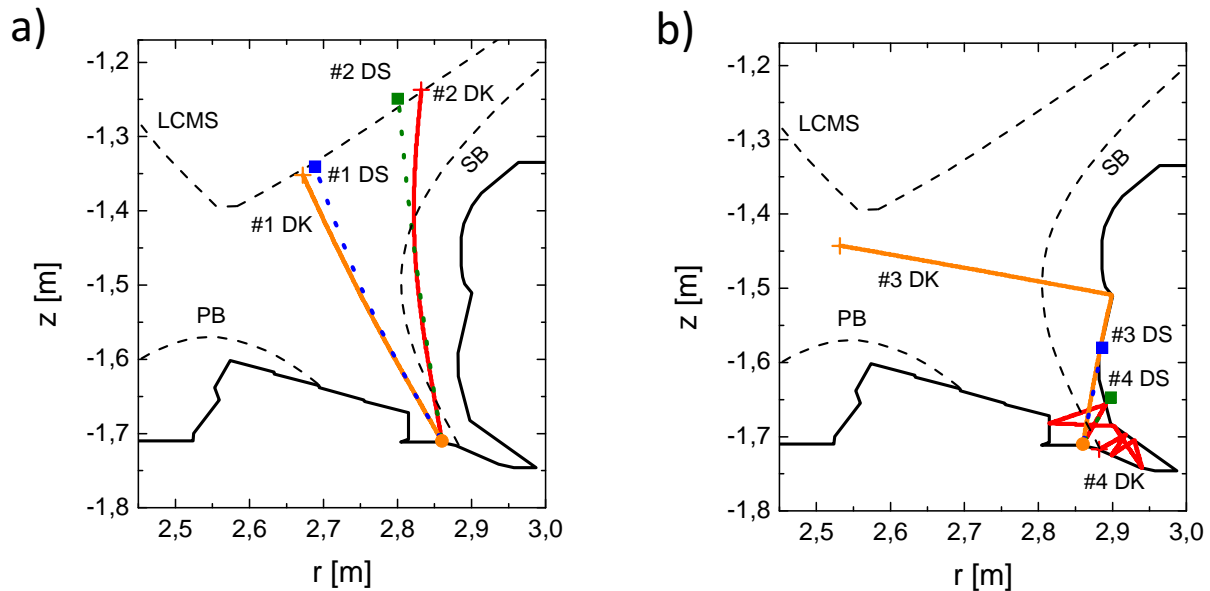
FIG. 5. Trajectories of 10 μm-radius W dust particles launched from JET outer divertor during the plasma pulse #82806 at 55-56 s, as predicted by DUSTTRACK (label "DK", solid lines) and DTOKS (label "DS", dotted lines). (a) shows the case of particles not intersecting the vessel: #1 (orange for DK and blue for DS) and #2 (red for DK and green for DS). (b) presents the trajectories of particles which impact on the vessel: #3 (orange for DK and blue for DS) and #4 (red for DK and green for DS). The common starting point is labeled with a full circle ($\bullet$) and the final points are marked with a plus sign ($+$) for DUSTTRACK and a full square ($\blacksquare$) for DTOKS, respectively. The contour of the JET divertor and the Last Closed Magnetic Surface ("LCMS" black dashed line) are also displayed, together with the SOL and Private Flux Region Boundaries ("SB" and "PB" black dashed lines) of the EDGE2D mesh.

(c-d), v_d (e-f) and χ_d (g-h). Pictures (a,c,e,g) refer to particles #1 and #2, pictures (b,d,f,h) refer to particles #3 and #4.

Starting with the particles which do not impinge on the vessel (#1 and #2, figure 5a), the comparison of trajectories (in terms of their shape and length) and lifetime (see the axis of time of figures 6a,c,e,g) shows another aspect of the substantial agreement between the two codes in describing the flight from an initial position to the separatrix where ablation occurs. This could be explained by the fact that the high power received by the dust grains approaching the separatrix rapidly brings T_d to W boiling temperature inducing a fast gas phase transition dynamics, even if surface evaporation is not taken into account by DTOKS (analogous to what obtained in section III for the higher T_e values, see figure 3). Relative to particles #1 and #2, DUSTTRACK estimates that the entire mass of particle #1 ablates (R_d goes to zero in figure 6c) through surface evaporation, before reaching W boiling temperature ($T_{boil} = 6203$ K, see figure 6a). Particle #2, instead, dies at T_{boil}. Minor differences between the trajectories #2 arise because DTOKS considers the space between the EDGE2D mesh and the vessel as a vacuum region (i.e. the region between the SOL Boundary, "SB" black dashed line in figure 5, and the contour of the wall).

Figure 6e shows a quite good agreement of the dust particles #1 and #2 velocity profiles up to the onset of their ablation, during which the fast decrease of M_d (figure 6c), with a similar force applied, leads to a steep rise

of the acceleration of the dust grains. The higher values of v_d evaluated by DTOKS at the end of their flight can be ascribed to the neglect of the surface evaporation as a mechanism for dust particles mass loss. Without the modeling of surface evaporation, the ablation process lasts indeed longer for DTOKS (e.g. 7 ms against 4 ms for particle #1) giving the time to the net force which acts on the dust grains to accelerate them to really high v_d.

Moving on to the trajectories which intersect the vessel, the absence of a module for dust-wall collisions in DTOKS has the consequence of prematurely removing dust particles before boiling temperature is reached, eventually underrating the length of the path travelled by the dust grains and finally their effective radiation emission important for TIEs. Two examples involving collisions are those of particles #3 and #4 (figure 5b). For DUSTTRACK, the reflection from one of the vertical divertor tiles drives particle #3 toward the inner chamber crossing the private region where it surface evaporates. Particle #4 gets trapped into the outer divertor leg because of multiple collisions with the wall. Due to the cool plasma there, T_d remains well below the melting temperature and no mass loss occurs. The particle dies once its normal reflection velocity is below the sticking limit of 1 m/s.

The effect of the dust-wall interaction model implemented in DUSTTRACK on the dust particles behavior is also appreciable considering the velocity profiles de-
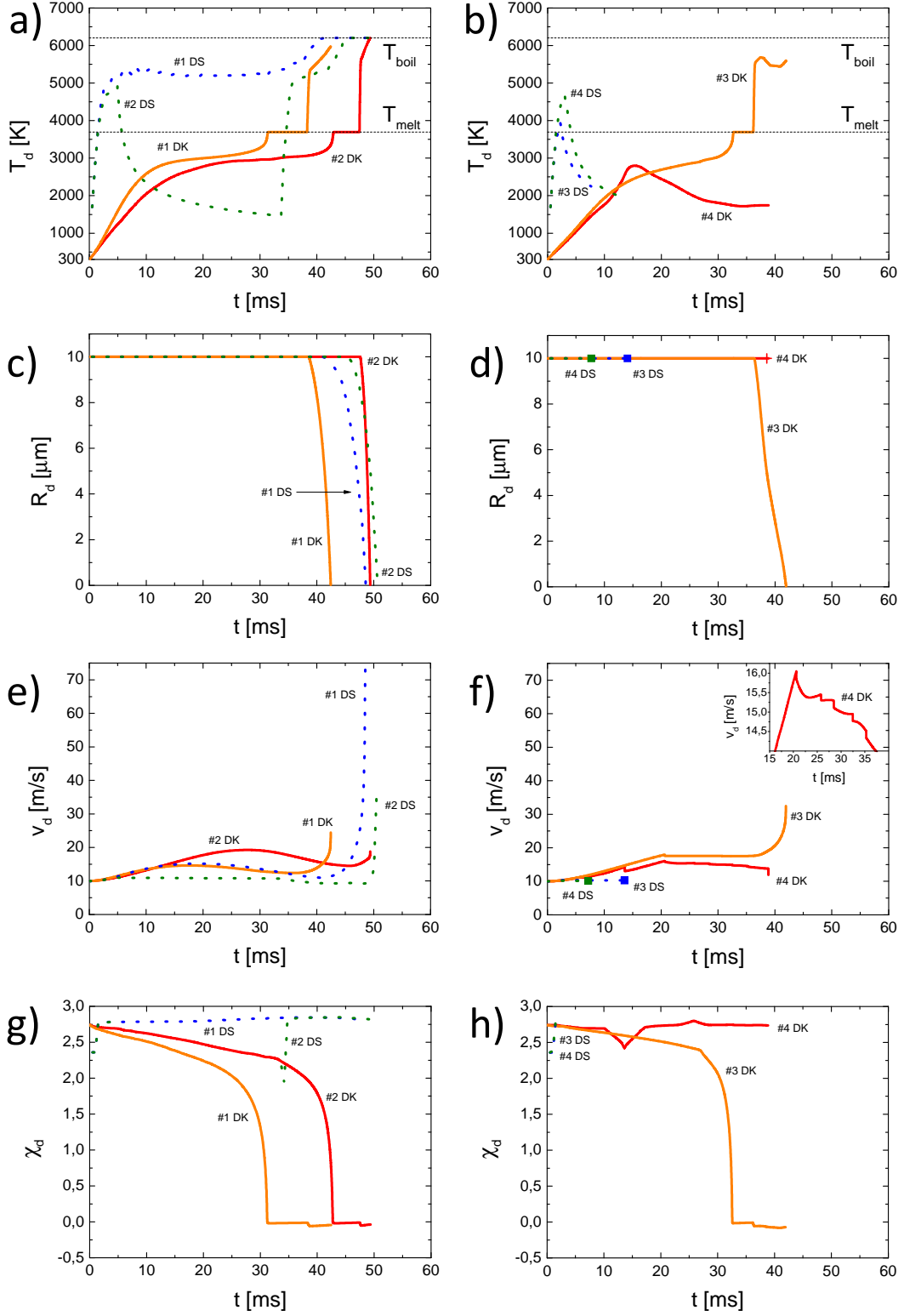
FIG. 6. Evolution of temperature T_d (a-b), radius R_d (c-d), velocity v$_d$ (e-f) and normalized potential χ_d (g-h) of test W dust particles ($R_{d,i} = 10\mu$m), launched with initial speed of 10 m/s from JET outer divertor, as predicted by DUSTTRACK (label "DK", solid lines) and DTOKS (label "DS", dotted lines). (a,c,e,g) present results for particles #1 and #2, (b,d,f,h) refer to particles #3 and #4. The color of the lines follows the scheme of figure 5.

picted in figure 6f. The collisions with the vessel of particles #3 and #4 lead to jump discontinuities in v_d, as a consequence of the inelastic character of the interactions. For both particles #3 and #4, the velocity loss after the collisions is small and sometimes is really hard to detect from the v_d profiles. In the upper panel of figure 6f, a zoom around the multiple collisions region of particle #4 is shown and the abrupt discontinuities in v_d are visible.

The main differences between the outputs of the two codes are the behaviors of T_d and χ_d (figures 6a-b and g-h). The steeper increase of the temperature estimated by DTOKS during the first few ms can be partly related to the consideration of neutral recombination of the plasma particles on the surface of the dust grain [6] as a further, and important, heating mechanism. The cooling of particles #2,#3,#4 predicted by DTOKS is merely due instead to the fact that they fall outside the EDGE2D mesh into the vacuum region. The extrapolation of the plasma profiles till the vessel, as implemented in DUST-TRACK, is thus necessary to more suitably estimate the evolution of T_d throughout dust particles lives.

As expected from the discussion in subsection II.1, the particles' normalized potential χ_d of DUSTTRACK particles, figures 6g-h, remains almost always positive, and is subject to a sharp decrease concurrently to the likewise stiff increase of T_d occurring when the particles try to escape from the divertor volume toward high T_e regions. Higher plasma and dust temperatures bring respectively to a growing importance of the SEE and TI emission terms thus increasing the incoming positive current and the dust electric potential. The steep increase of T_d during the first ms for DTOKS particles rapidly leads to a positive charge on dust particles' surface. This results in the onset of the semi-empirical shielding model (subsection II.1) and χ_d remains in the range $2.5 \div 3$. The great difference between χ_d at the end of the lifetime of particles #1 and #2 highlights the need for a refinement of the charge model of DUSTTRACK.

V. CONCLUSIONS

Efficient particles tracking codes, DTOKS and DUST-TRACK, have been developed to allow studies and simulation of isolated dust particles dynamics in plasmas of tokamaks.

The comparison between the two codes has been successfully performed, giving confidence that both codes are suitable tools for studies of dust mobilization and plasma contamination. An indirect cross-check of predicted dust trajectories and parameters with real tokamak data from existing diagnostics should finally highlight the correlation between dust dynamics and some tokamak physics phenomena like Transient Impurity Events (TIEs).

Some conclusions can be schematically drawn from the results of the comparison:

1. The charging models of DTOKS and DUST-TRACK predict the same results for negative charged dust particles. The dust particles positive potential shielding for $\delta \approx 1$ and $\delta > 1$ (due to the electron cloud emitted by the dust particles) is semi-empirically described in DTOKS and not fully considered in DUSTTRACK, which admits also dust particles with a slightly positive potential.

2. The numerical comparison of the collection drag forces in DTOKS and DUSTTRACK appears satisfactory.

3. The orbital forces (Coulomb scattering of ion particles by dust grains) are evaluated by the somewhat different expressions in the two codes, approaching alike values for plasma drift velocity well below plasma thermal velocity.

4. The sensitivity analysis carried out on DTOKS and DUSTTRACK highlights the importance of surface evaporation for the estimate of the distance travelled by and the lifetime of the dust particles.

5. The comparison of the output of the two codes applied to a JET plasma pulse shows a satisfactory agreement between the predicted trajectories (both in terms of shape and length) and lifetime of dust particles not intersecting the vessel.

The basis objective of this work consists in the cross-validation of the physics models of the codes DUST-TRACK and DTOKS, fruitful in the study of dust dynamics in tokamaks. The use of independent approaches, summarized in table I, gives confidence that application to the analysis of experimental data can be performed reliably and, at the same time, a basis has been provided to the developers of simulation codes.

[1] G. F. Matthews, J. Nucl. Mater. **438, Supplement**, S2 (2013).

[2] M. Sertoli, J. C. Flanagan, M. Bacharis, O. Kardaun, A. Jarvinen, G. F. Matthews, S. Brezinsek, D. Harting,

A. Cackett, E. Hodille, I. H. Coffey, E. Lazzaro, and T. Pütterich, J. Nucl. Mater. **463**, 837 (2015).

[3] J. C. Flanagan, M. Sertoli, M. Bacharis, G. F. Matthews, P. C. de Vries, A. Widdowson, I. H. Coffey, G. Arnoux, B. Sieglin, S. Brezinsek, J. W. Coenen, S. Marsen, T. Craciunescu, A. Murari, D. Harting, A. Cackett, and E. Hodille, Plasma Phys. Contr. F. **57**, 014037 (2015).

[4] E. Lazzaro, I. Proverbio, F. Nespoli, S. Ratynskaia, C. Castaldo, U. deAngelis, M. DeAngeli, J.-P. Banon, and L. Vignitchouk, Plasma Phys. Contr. F. **54**, 124043 (2012).

[5] M. Bacharis, M. Coppins, and J. E. Allen, Phys. Rev. E **82**, 026403 (2010).

[6] M. Bacharis, M. Coppins, and J. E. Allen, Phys. Plasmas **17**, 042505 (2010).

[7] J. E. Allen, Phys. Scripta **45**, 497 (1992).

[8] P. K. Shukla and A. A. Mamun, *Introduction to Dusty Plasma Physics*, Series in Plasma Physics and Fluid Dynamics (CRC Press, 2001).

[9] R. A. Langley, J. Bohdansky, W. Eckstein, P. Mioduszewski, J. Roth, E. Taglauer, E. W. Thomas, H. Verbeek, and K. L. Wilson, Nucl. Fusion **24**, S9 (1984).

[10] E. W. Thomas, Vienna: IAEA , 94 (1984).

[11] M. S. Chung and T. E. Everhart, J. Appl. Phys. **45**, 707 (1974).

[12] S. Dushman, Rev. Mod. Phys. **2**, 381 (1930).

[13] A. H. W. Beck, *Thermionic Valves* (Cambridge University Press, 2015).

[14] G. L. Delzanno, G. Lapenta, and M. Rosenberg, Phys. Rev. Lett. **92**, 035002 (2004).

[15] G. L. Delzanno, A. Bruno, G. Sorasio, and G. Lapenta, Phys. Plasmas **12**, 062102 (2005).

[16] *ITER Technical Basis, ITER EDA Documentation Series No 24, IAEA, Vienna 2002*.

[17] R. Marek and J. Straub, Int. J. Heat Mass Tran. **44**, 39 (2001).

[18] A. T. Dinsdale, Calphad **15**, 317 (1991).

[19] D. R. Lide, *CRC Handbook of Chemistry and Physics 80th Edition* (Taylor & Francis, 1999).

[20] R.D. Smirnov, A.Yu. Pigarov, M. Rosenberg, S.I. Krasheninnikov, D.A. Mendis, Plasma Phys. Contr. F. **49**, 347 (2007).

[21] M. S. Barnes, J. H. Keller, J. C. Forster, J. A. O'Neill, and D. K. Coultas, Phys. Rev. Lett. **68**, 313 (1992).

[22] S. A. Khrapak, A. V. Ivlev, S. K. Zhdanov, and G. E. Morfill, Phys. Plasmas **12**, 042308 (2005).

[23] I. H. Hutchinson, Plasma Phys. Contr. F. **48**, 185 (2006).

[24] V. E. Fortov, A. V. Ivlev, S. A. Khrapak, A. G. Khrapak, and G. E. Morfill, Phys. Rep. **421**, 1 (2005).

[25] S. Chandrasekhar, Astrophys. J. **97**, 255 (1943).

[26] E. Lazzaro, S. Ratynskaia, and I. Proverbio, AIP Conf. Proc. **1392**, 103 (2011).

[27] L. Vignitchouk, P. Tolias, and S. Ratynskaia, Plasma Phys. Contr. F. **56**, 095005 (2014).

[28] S. Ratynskaia, L. Vignitchouk, P. Tolias, I. Bykov, H. Bergsåker, A. Litnovsky, N. den Harder, and E. Lazzaro, Nucl. Fusion **53**, 123002 (2013).

[29] S. Ratynskaia, P. Tolias, A. Shalpegin, L. Vignitchouk, M. De Angeli, I. Bykov, K. Bystrov, S. Bardin, F. Brochard, D. Ripamonti, N. den Harder, and G. De Temmerman, J. Nucl. Mater. **463**, 877 (2015).

[30] C. Thornton and Z. Ning, Powder Technol. **99**, 154 (1998).

[31] W. Goldsmith, *Impact: the theory and physical behaviour of colliding solids* (London: E. Arnold, 1960).

[32] X. Li, P. F. Dunn, and R. M. Brach, Aerosol Sci. Tech. **33**, 376 (2000).

[33] R. Bridson, R. Fedkiw, and J. Anderson, ACM T. Graphic. **21**, 594 (2002).

[34] M. C. van Beek, C. C. M. Rindt, J. G. Wijers, and A. A. van Steenhoven, Powder Technol. **165**, 53 (2006).

[35] A. E. Jaervinen, M. Groth, M. Airila, P. Belo, M. Beurskens, S. Brezinsek, M. Clever, G. Corrigan, S. Devaux, P. Drewelow, T. Eich, C. Giroud, D. Harting, A. Huber, S. Jachmich, K. Lawson, B. Lipschultz, G. Maddison, C. Maggi, T. Makkonen, C. Marchetto, S. Marsen, G. F. Matthews, A. G. Meigs, D. Moulton, M. F. Stamp, S. Wiesen, M. Wischmeier, and JET-EFDA collaborators, J. Nucl. Mater. **463**, 135 (2015).

[36] R. Simonini, G. Corrigan, G. Radford, J. Spence, and A. Taroni, Contrib. Plasm. Phys. **34**, 368 (1994).

[37] D. Shepard, in *Proceedings of the 1968 23rd ACM National Conference* (ACM, New York, NY, USA, 1968) pp. 517–524.